JOURNAL OF CATALYSIS 73, 136–146 (1982)

Surface Electronic Properties and CO Hydrogenation Activity of Nickel Deposited on Rutile TiO_2(100) as a Model Supported Catalyst

CHIA-CHIEH KAO, SHOU-CHIN TSAI, AND YIP-WAH CHUNG

Department of Materials Science and Engineering, Northwestern University, Evanston, Illinois 60201

Received June 22, 1981; revised September 14, 1981

A combined ultrahigh-vacuum surface analysis-high-pressure cell system has been used to study the electronic properties and CO hydrogenation behavior of nickel deposited on single-crystal rutile TiO_2(100) as a model supported catalyst. Photoemission studies show that nickel atoms at the Ni/TiO_2(100) interface are negatively charged. *In situ* CO hydrogenation studies at a total pressure of 80 Torr have been performed on Ni/TiO_2(100) and Ni(111) from 170 to 270°C. The methane turnover number of Ni/TiO_2(100) is a function of the Ni coverage and attains a maximum at an average Ni thickness of 5 Å. the methanation activity of 5 Å Ni/TiO_2 is a factor 3.3–3.7 times that of Ni(111), with an accompanying shift of the product distribution toward higher hydrocarbons.

INTRODUCTION

In heterogeneous catalysis, the support is primarily used as a means of dispersing the metal catalyst over a large surface area. But early studies by Schwab and co-workers (*1, 2*), Szabo and Solymosi (*3, 4*), and Baddour and Deibert (*5*) on formic acid decomposition using differently supported Ni catalysts showed that the activity depends on the electron concentration of the support. Recently, Tauster *et al.* (*6–8*) showed that strong metal–support interaction (SMSI) exists for group VIII metals supported on several binary oxides. For example, for titania-supported catalysts, they were well dispersed as evidenced by TEM and X-ray diffraction measurements; yet the H_2 and CO chemisorptions were largely suppressed (*6*). Vannice and co-workers (*9–11*) and Bartholomew and co-workers (*12–13*) found similar phenomena in the Ni/TiO_2 system. In addition, the methane yield of Ni/TiO_2 was found to increase by an order of magnitude over that of unsupported nickel or nickel on other supports (*9, 10, 13*). Recent theoretical studies by Horsley (*14*) on the Pt/TiO_2 system suggested that this SMSI state could be the result of charge transfer between the metal atom and the substrate titanium cation. There is some experimental evidence for this charge transfer behavior for several metal-oxide systems (*15, 16*).

To elucidate further the correlation between catalytic behavior and charge transfer, we adopted the approach of the study of model systems (*17*), in which one prepares model metal–support systems that have well-defined interfacial structure and composition and performs *in situ* probe reactions on these well-defined model systems so that one can uncover the correlation between catalytic behavior (activity, product distribution, and poison resistance) and interfacial properties. The general philosophy of this approach can be achieved by incorporating a high-pressure (1–100 atm) reaction cell into an ultrahigh-vacuum (UHV) surface analytical system. Somorjai and co-workers (*17–21*), the NBS group (*22–25*), and Krebs and Bonzel (*26–28*) have built and used such systems to investigate CO hydrogenation reactions over small-area (~1 cm^2) catalysts. Good agreement was often found with data obtained from dispersed catalysts (*18, 24, 26*). The ability to modify the surface in a controlled manner and to closely monitor the conditions of the surface before and after the

0021-9517/82/010136-11$02.00/0
Copyright © 1982 by Academic Press, Inc.
All rights of reproduction in any form reserved.

reaction is an important asset of this approach.

In this paper, we report the electronic properties and CO hydrogenation activity of nickel deposited on single-crystal TiO_2(100) surfaces, using the clean Ni(111) surface as a reference. To simulate the conditions leading to the observed SMSI in titania-supported catalysts (*6, 7*), all TiO_2(100) single crystals were reduced by heating at 400°C for 20 h. The Ni/TiO_2(100) model catalysts so prepared demonstrated catalytic behavior remarkably different from that of Ni(111).

EXPERIMENTAL

The experimental system used in this study was a Physical Electronics PHI 548 ESCA/Auger analysis system with a base pressure in the low 10^{-10}-Torr range and capable of ion sputtering, Auger electron spectroscopy (AES), low-energy electron diffraction (LEED), and photoemission using the AlKα($h\nu$ = 1486.6 eV) and He (21.2, 40.8 eV) lines.

Single crystals of Ni(111) and rutile TiO_2(100) used in these experiments were circular disks ~1 cm diameter and 1 mm thick, prepared by standard metallographic techniques (*29*) to give an orientation accuracy of better than 1° and a surface smoothness of 1/4 μm. The sample was mounted on a ceramic holder with a 2-mil-thick tantalum heater foil attached immediately behind the crystal. A Chromel–Alumel thermocouple was pressure contacted to the front surface of the crystal for temperature measurements. The sample holder sat in a ceramic "parking lot" on the specimen manipulator stage and held on the "parking lot" by four spring contacts made of Be–copper and thermocouple materials through which heater currents were passed and temperature measurements made, respectively.

Bulk impurities (in particular, sulfur) from the Ni crystal were first removed by repetitive cycles of heating at 600°C and Ar-ion sputtering. The normal cleaning procedure before any experiment was sputtering at 520°C with 2-kV Ar-ion beam of several microamperes per square centimeter for 10 min, followed by annealing at 520°C for 10 min. This procedure generally produced a clean ordered surface, as evidenced by the absence of impurities detectable by AES and the occurrence of a sharp LEED pattern characteristic of the Ni(111) surface.

All TiO_2 crystals used in our experiments were first reduced by heating under vacuum at 400°C for 20 h. This treatment produced a conducting n-type TiO_2 crystal due to the loss of oxygen. A clean TiO_2(100) crystal surface was obtained by Ar sputtering and subsequent annealing at 400°C for 10 min. A (1 × 3) LEED pattern (*30, 31*) was obtained from this surface. Nickel deposition onto the TiO_2 surface was done via a resistively heated tungsten evaporator at a substrate temperature of 120–140°C. A mask in front of the evaporator defined the deposition to the central part of the TiO_2 crystal with an area of 0.380 cm^2. The average Ni coverage was calculated from the attenuation of the Ti $2p_{3/2}$ and O 1s peaks and also from the increase of the Ni $2p_{3/2}$ peak intensity, assuming their mean free paths to be $\lambda_{Ti\ 2p}$ = 15.0 Å, $\lambda_{O\ 1s}$ = 14.6 Å, and $\lambda_{Ni\ 2p}$ = 12.8 Å. Good agreement was found between these calculations.

In measuring the energy positions of the Ni $2p_{3/2}$ core level and the Ni $L_3M_{2,3}M_{2,3}$ Auger transition, a piece of Au foil was placed in contact with the TiO_2 crystal, and the Au $4f_{7/2}$ peak with a binding energy of 83.8 eV was used as the energy reference. All photoemission spectra were taken with a PHI model 15-250G double-pass cylindrical-mirror analyzer operating in the large-aperture mode ($\Delta E/E$ = 1.2%) and at a pass energy of 25 eV for the core level spectra and 50 eV for the Ni $L_3M_{2,3}M_{2,3}$ Auger spectra.

For *in situ* CO hydrogenation studies, an isolation cell was attached to the UHV chamber as shown in Fig. 1. It was a stainless-steel six-way cross capable of operating from ultrahigh vacuum to pressures ~2

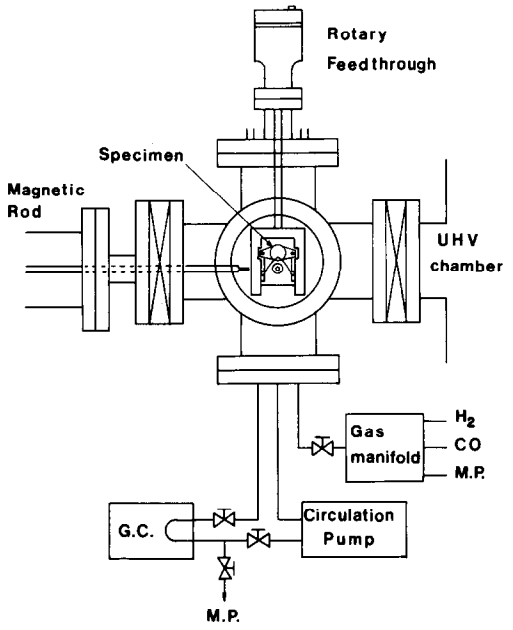

FIG. 1. The isolation cell setup. The specimen to be studied is first prepared and characterized in the UHV chamber. Then it is retracted into the isolation cell using a magnetically coupled rod. The isolation cell can be pressurized up to 2 atm with the reactant gases. The products can be analyzed by gas chromatography. At the conclusion of the high-pressure experiment, the cell can be evacuated, and the specimen can be reintroduced into the UHV chamber for surface analysis.

atm. The inside wall of the cell was coated with gold to minimize contamination from the cell, background reaction, and adsorption of product gasses onto the wall. The isolation cell was equipped with a "parking-lot" assembly similar to that in the UHV chamber. The specimen could be transferred between the UHV chamber and the isolation cell via a magnetically coupled rod. This arrangement allowed us to perform sequential surface preparation and characterization inside the UHV chamber and high-pressure (up to 2 atm) catalysis experiments inside the isolation cell. During catalytic reaction studies, all gate valves were closed to isolate the cell from the UHV chamber and the magnetically coupled rod. A reaction cell volume of ~300 ml was enclosed. At the end of a high-pressure catalysis experiment, the isolation cell could be evacuated sequentially by a mechanical pump, a sorption pump, and an ion pump. The pumpdown time from 1 atm to 1×10^{-8} Torr was less than 3 min.

Research-grade hydrogen (99.9995%) and carbon monoxide (99.99%) were obtained from the Matheson Company. Carbon monoxide was passed through a trap at liquid nitrogen temperature to remove traces of iron carbonyls. Synthesis gas with a H_2/CO ratio of 3/1 was first mixed in the gas manifold and then expanded into the isolation cell to give $P_{H_2} = 60$ Torr and $P_{CO} = 20$ Torr. The gas pressure was monitored by a Viatran transducer absolute pressure gauge.

A circulation pump was used for stirring the gas inside the cell. However, we found that this stirring was not critical with a total conversion of less than 3×10^{-5} under our normal reaction conditions. Product yields and distributions were determined using a Hewlett–Packard 5711A GC with dual flame ionization detector. The columns were 1/8-in.-o.d. × 10-ft stainless-steel tubes packed with 80- to 100-mesh Poropak Q and were kept at 100°C. Air and H_2 for the ionization detector and He carrier gas were all zero grade with low hydrocarbon content (<2.0 ppm CH_4 for air and <0.5 ppm CH_4 for H_2 and He). The gas sampling valve was a Carle 4018 microvolume valve with 1-cm³ gas sampling loop. It was surrounded by a purged He jacket to minimize air leakage through the valve into the reaction cell. Each sampling consumed 3 cm³ of gas which was 1% of the isolation cell volume and should not affect the reaction and product yield calculations appreciably. The output from the ionization detector was amplified to give a sensitivity of 3×10^{-6} Torr for methane or less than 4% of a monolayer of methane from a surface of 0.380 cm². After the catalytic reaction, the cell was evacuated and the specimen cooled and transferred back into the UHV chamber where the surface was checked by Auger electron spectroscopy.

RESULTS

Nickel Deposition onto $TiO_2(100)$

The He I ultraviolet photoemission spectra for different Ni coverages θ on the $TiO_2(100)$ surface are shown in Fig. 2. There are three major peaks located at -4.9, -6.1, and -7.5 eV in the valence band relative to E_F for the clean $TiO_2(100)$ surface. The emission from the -4.9-eV peak is attenuated faster than those at -6.1 and -7.5 eV with increased Ni coverage. These peak positions relative to E_F remain constant, indicating no band bending change on the TiO_2 crystal surface with Ni deposition. The density of states at $E_F = 0$ is relatively low at coverages less than $\theta =$ 2 Å and increases thereafter with the Ni coverage.

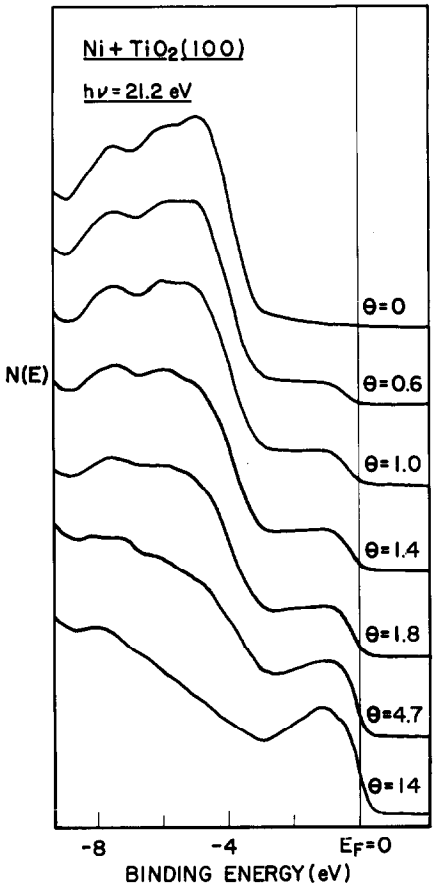

FIG. 2. The He I UPS spectra for different Ni coverages θ and the $TiO_2(100)$ surface. Here θ is in angstroms.

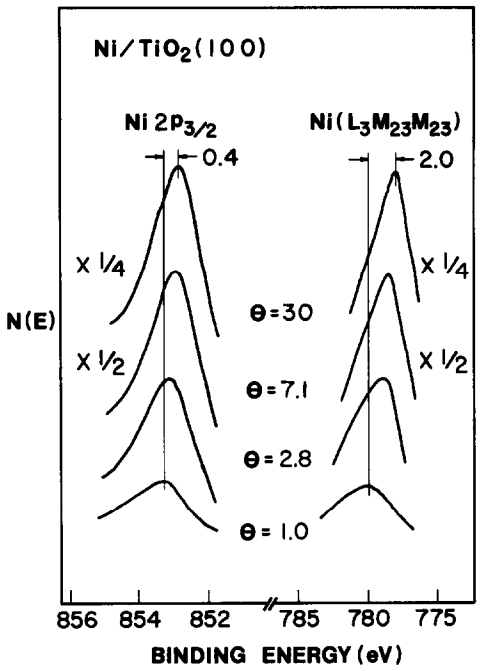

FIG. 3. The Ni $2p_{3/2}$ peak and the Ni $L_3M_{2,3}M_{2,3}$ Auger peak for Ni deposited on the $TiO_2(100)$ surface as a function of Ni coverage θ.

Figure 3 shows the evolution of the Ni $2p_{3/2}$ core level and the Ni $L_3M_{2,3}M_{2,3}$ Auger transition with increasing Ni coverage θ on the $TiO_2(100)$ surface. The Ni $2p_{3/2}$ peak shifts toward smaller binding energy by 0.4 eV as the Ni coverage increases from 1.0 to 30 Å. This is accompanied by a Ni Auger peak shift of 2.0 eV toward smaller binding energy, i.e., higher kinetic energy. The energy positions of the Ni $2p_{3/2}$ and the Auger transition at $\theta = 30$ Å are essentially identical to those of bulk Ni, as expected from the short mean free paths of photoelectrons in this energy range. Therefore, relative to bulk Ni, the 1.0 Å of Ni at the $Ni/TiO_2(100)$ interface has a Ni $2p_{3/2}$ binding energy shift (ΔBE) of $+0.4 \pm 0.05$ eV (the + sign indicates an increase in the binding energy) and a Ni Auger kinetic energy shift of -2.0 ± 0.1 eV (the $-$ sign indicates a decrease in the Auger kinetic energy).

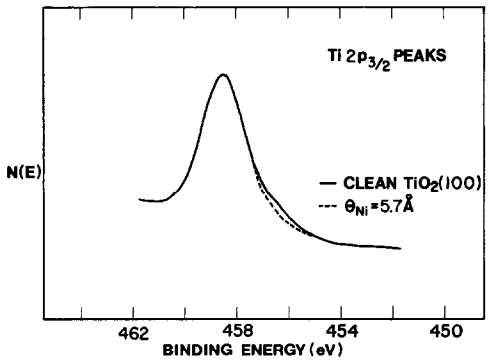

FIG. 4. The Ti $2p_{3/2}$ peak from the clean ordered $TiO_2(100)$ surface before and after the deposition of 5.7 Å of Ni. Different vertical scales are used such that both peaks have the same peak height.

Figure 4 shows the Ti $2p_{3/2}$ peak from the sputtered and subsequently annealed $TiO_2(100)$ surface and the same surface after the deposition of 5.7 Å of Ni. Different vertical scales are used such that these two peaks have the same peak height. On the clean $TiO_2(100)$ surface, in addition to the peak at a binding energy of 458.5 eV, there is a shoulder at a binding energy of 456.4 eV. Deposition of 5.7 Å of Ni removes the shoulder at 456.4 eV.

Figure 5 shows the evolution of the Ni (61 eV) Auger peak height as a function of heating time at 210°C after the deposition of 5 Å Ni onto a clean ordered $TiO_2(100)$ surface. Because of the short mean free path of the Ni (61 eV) Auger electrons (4–5 Å), this curve can represent fairly the variation in the number of surface Ni atoms as a function of time. The decrease in the Ni (61 eV) Auger peak intensity is rapid at the beginning and slows down after 5 min. The Ni (61 eV) Auger signal decreases to 88% of its initial value after 1 h of heating at 210°C.

After the deposition of about 20 Å of Ni on the clean $TiO_2(100)$ surface at a substrate temperature of 140°C and a rate of 2 Å/min, a blurred hexagonal LEED pattern was observed. It became a sharp hexagonal LEED pattern characteristic of Ni(111) after annealing at 190°C for 2 min.

CO Hydrogenation Reactions

Catalytic CO hydrogenation reactions were performed on both Ni(111) and Ni-covered $TiO_2(100)$ surfaces at $P_{H_2} = 60$ Torr and $P_{CO} = 20$ Torr. A typical plot for the production of methane from Ni(111) at 200°C as a function of time is shown in Fig. 6. The reaction rate was high in the first 10 min and slowed down thereafter. The initial slope was taken to calculate the methane turnover number (TON), assuming a nickel packing density of $1.86 \times 10^{15}/cm^2$. The methane TONs over the Ni(111) surface from 170 to 270°C were then plotted in Arrhenius form in Fig. 7. The slope of the line corresponds to an activation energy of 26.7 ± 0.9 kcal/mole.

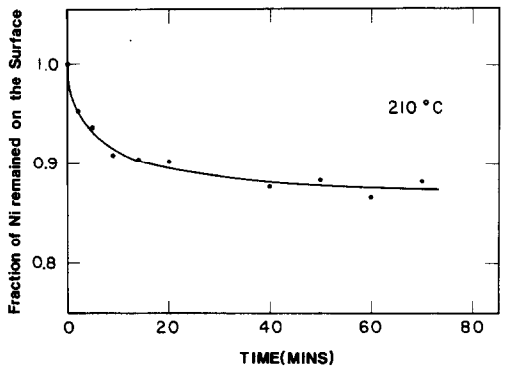

FIG. 5. The variation of the Ni (61 eV) Auger peak height as a function of heating time at 210°C after the deposition of 5 Å Ni onto a clean ordered $TiO_2(100)$ surface.

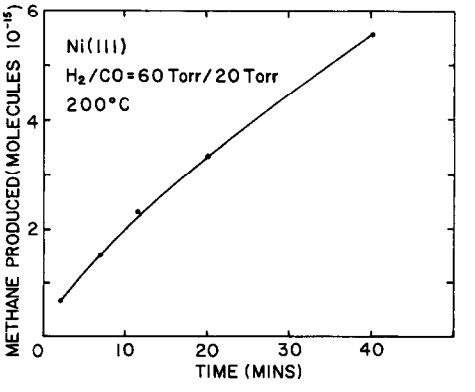

FIG. 6. The number of methane molecules produced from a Ni(111) catalyst (area ~0.66 cm^2) as a function of reaction time. $P_{H_2} = 60$ Torr, $P_{CO} = 20$ Torr, $T = 200$°C.

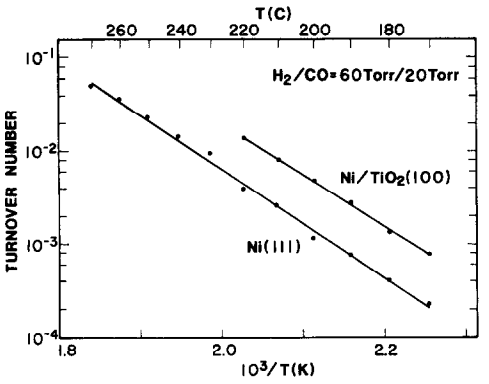

FIG. 7. Arrhenius plots of the methane turnover number for Ni(111) and 5 Å $Ni/TiO_2(100)$. P_{H_2} = 60 Torr, P_{CO} = 20 Torr.

When Ni-deposited $TiO_2(100)$ surface was used as the catalyst, the CH_4 yield varied as a function of the Ni coverage, as shown in Fig. 8. At a temperature of 190°C, the methane yield increases with the average Ni thickness at lower Ni coverage. It reaches a maximum at an average Ni coverage of 5 Å and then approaches the value obtained from the Ni(111) surface at larger thickness. An Arrhenius plot of the methane TONs over the 5 Å Ni-covered $TiO_2(100)$ surface was included in Fig. 7. The TON was calculated assuming that the Ni surface concentration is $1.86 \times 10^{15}/cm^2$ (i.e., same as Ni(111)). The methane yields from the $Ni/TiO_2(100)$ surface are ~3.3–3.7 times that from the Ni(111) surface over the temperature range 170 to 220°C. The activation energy for methane production from the $Ni/TiO_2(100)$ surface is 25.2 ± 0.6 kcal/mole. It should be noted that all the data points shown in Fig. 7 are generally reproducible to within 15% over a period of several months. Also blank experiments show that the isolation cell has a negligible background reactivity, pointing to the effectiveness of the gold coating.

The enhancement of the methanation activity of $Ni/TiO_2(100)$ is accompanied by a change in product distributions. Figures 9 and 10 display the product distributions over the Ni(111) surface and the 5 Å Ni-covered $TiO_2(100)$ surface as a function of temperature, respectively. The ethylene, ethane, and propylene yields are normalized to the methane yield at each temperature (operation at a GC column temperature of 100°C limited our hydrocarbon detection up to C_3 products only). One observes a general shift of the product distribution toward higher hydrocarbons. For example,

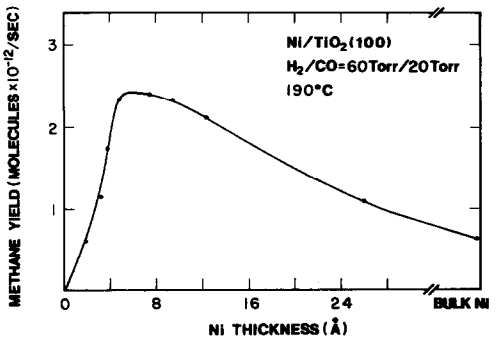

FIG. 8. The methane yield from $Ni/TiO_2(100)$ as a function of the average Ni thickness. P_{H_2} = 60 Torr, P_{CO} = 20 Torr, T = 190°C.

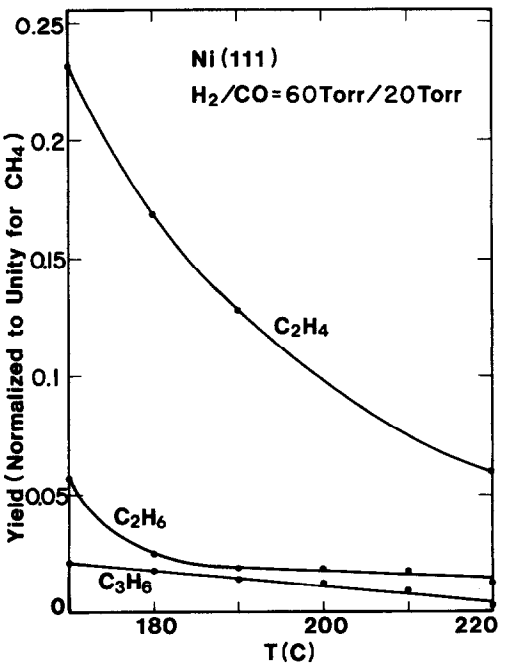

FIG. 9. Product distribution (normalized to CH_4) for the CO hydrogenation reaction over the Ni(111) surface. P_{H_2} = 60 Torr, P_{CO} = 20 Torr.

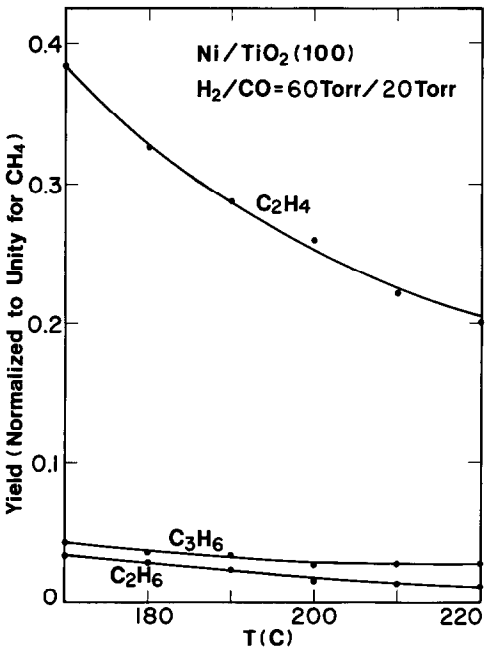

FIG. 10. Product distribution (normalized to CH_4) for the CO hydrogenation reaction over the 5 Å $Ni/TiO_2(100)$ surface. P_{H_2} = 60 Torr, P_{CO} = 20 Torr.

on the Ni(111) surface, the ethylene yield is 6% of methane at 220°C, while on the $Ni/TiO_2(100)$ surface at the same temperature, the ethylene yield is 20% of methane.

The Auger spectra from the Ni(111) surface after the CO hydrogenation reaction at 200°C for 1 h are shown in Fig. 11. The spectrum just after the reaction shows a carbon peak at 275 eV and an oxygen peak at 510 eV. After flashing to 300°C to remove the chemisorbed CO, the carbon peak shape changes to that of a surface carbide (*24, 26, 27*) and the oxygen peak disappears. The $Ni/TiO_2(100)$ surface after the reaction always shows a carbon peak with the same shape as that from the flashed Ni(111) surface in Fig. 11 irrespective of whether the surface is flashed or not.

DISCUSSION

Nickel Deposition onto $TiO_2(100)$

A method was developed recently to estimate roughly the chemical shift associated with core levels and the corresponding amount of charge transfer at a metal–semiconductor interface (*16, 29*). The binding energy shift (ΔBE) of the core level relative to the Fermi level can be written as

$$\Delta BE = \Delta E - \Delta R + \Delta E_{\text{bending}}, \quad (1)$$

where ΔE is the chemical shift due to changes in the initial-state charge distribution, ΔR the relaxation shift, and $\Delta E_{\text{bending}}$ band bending shift. Similarly, the core–core–core Auger kinetic shift (ΔK) can be expressed as

$$\Delta K = -\Delta E + 3\Delta R - \Delta E_{\text{bending}}. \quad (2)$$

Equation (2) is derived by assuming that the chemical shifts of the three core levels involved are the same (*32*) and that the final-state two-hole relaxation energy is $2\Delta R$ (*33, 34*). Therefore, by measuring the binding energy shift for a given core level, the Auger kinetic energy shift, and the band

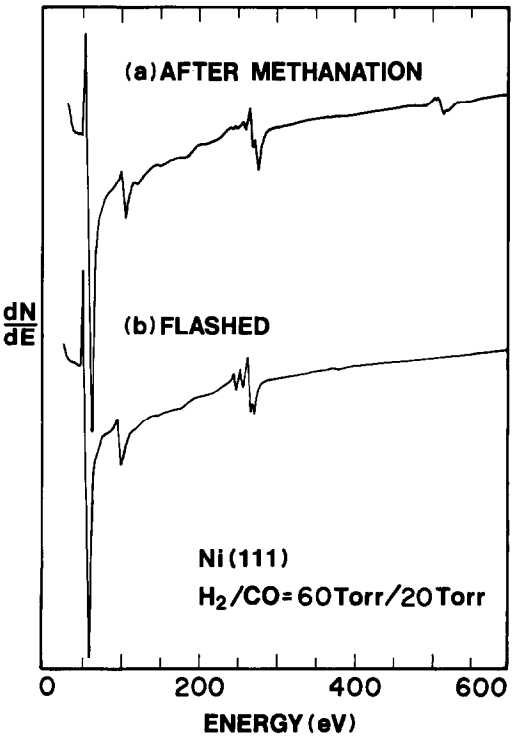

FIG. 11. Auger spectra from the Ni(111) surface (a) after the CO hydrogenation reaction at 200°C for 1 h, and (b) the same surface after flashing to 300°C.

bending, one can calculate the chemical shift of the core level with Eqs. (1) and (2).

For 1.0 Å of Ni on $TiO_2(100)$, we found ΔBE to be $+0.4 \pm 0.05$ eV for the Ni $2p_{3/2}$ core level, ΔK to be -2.0 ± 0.1 eV for the Ni $L_3M_{2,3}M_{2,3}$ Auger peak, and $\Delta E_{\text{bending}}$ to be 0.0 ± 0.05 eV relative to 30 Å of Ni (bulk). Using Eqs. (1) and (2), one can show that $\Delta E = -0.4$ eV and $\Delta R = -0.8$ eV. The negative chemical shift of 1.0 Å of Ni on $TiO_2(100)$ relative to bulk Ni indicates that Ni atoms on the $TiO_2(100)$ surface are negatively charged. Therefore, *there is an electron transfer from TiO_2 to Ni.* From the empirical correlation between the Ni core level shift and the charge on the Ni atom for several Ni compounds (*29*), one can roughly estimate the charge transfer to be ~0.1 electron per Ni atom. Similar results (*29*) were found for Ni on $TiO_2(110)$. Note that these electrons cannot be derived from the TiO_2 bulk as this will result in the creation of a depletion region and thus an upward band bending near the TiO_2 surface. No detectable band bending changes were observed by ultraviolet photoelectron spectroscopy (UPS).

After argon sputtering and annealing of the $TiO_2(100)$ surface, a weak shoulder appears on the lower-binding energy side of the Ti $2p_{3/2}$ peak, as shown in Fig. 4. This shoulder is due to the existence of Ti^{3+} species, produced as a result of reduction of the TiO_2 surface (*8, 16, 29, 31, 35, 36*). These lower-oxidation-state Ti species were removed after the Ni deposition, as evidenced by the disappearance of the shoulder. This observation suggests that the negative charge on the Ni atoms may be derived from these Ti^{3+} species. This is also consistent with the result of Horsley's calculation (*14*) on the Pt/TiO_2 system in which he found that an appreciable electron transfer from Ti to Pt takes place only when Ti is in a reduced state.

The Ni atoms deposited on the $TiO_2(100)$ surface are well dispersed at low coverage as evidenced from the absence of emission at the Fermi level at 1.0 Å coverage in the UPS spectrum (Fig. 2). On heating, the number of surface Ni atoms decreases as shown in Fig. 5. The initial rapid decrease of the Ni (61 eV) Auger signal is probably due to the sintering of Ni surface atoms (*37, 38*). After about 5 min, the Ni signal decrease slows down. This is likely due to a combination of the lower sintering rate of larger Ni clusters and diffusion of Ni into bulk TiO_2 (*29*).

CO Hydrogenation Reactions

The kinetic data for methanation on Ni(111) at $P_{H_2} = 60$ Torr and $P_{CO} = 20$ Torr agree with those on the Ni(100) surface (*24*) and Ni dispersed on Al_2O_3 (*39, 40*) to better than 20% over the temperature range 170–270°C. The product distributions are also similar. For example, at 1 atm, 230°C, and $\frac{4}{1}$ H_2/CO, the Ni(100) surface yields a C_2/C_1 ratio of ~6% (*24*). The C_2/C_1 ratio for 5% Ni/Al_2O_3 at 1 atm, 235°C, and $\frac{3}{1}$ H_2/CO was found by Vannice (*40*) to be ~10%. The corresponding ratio for the Ni(111) surface at 80 Torr, 220°C, and $\frac{3}{1}$ H_2/CO is 8% (Fig. 9).

Compared to Ni(111), the $Ni/TiO_2(100)$ catalyst shows a higher specific activity for the CO hydrogenation reaction. Similar effects were observed by Vannice and Garten (*9, 10*) and Bartholomew *et al.* (*12*). Both groups had difficulties in calculating the specific activity because the surface area cannot be estimated from H_2 and CO chemisorption due to the suppression of H_2 and CO chemisorption on Ni/TiO_2 catalysts. However, even on a per gram basis (*9*) or based on transmission electron microscopy measurements (*12*), the specific activity of Ni/TiO_2 was estimated to be about an order of magnitude higher than that of unsupported Ni and Ni/SiO_2. In our studies, all turnover numbers shown in Fig. 7 were calculated from the measured geometrical area of the evaporated Ni overlayer (0.380 cm^2), assuming a nickel surface concentration of 1.86×10^{15} atoms/cm^2. The methanation activity of 5 Å $Ni/TiO_2(100)$ is about 3.3–3.7 times that of Ni(111), with a shift of the

product distribution toward higher hydrocarbons. At 80 Torr, $\frac{3}{1}$ H_2/CO, and 200°C, $Ni/TiO_2(100)$ yields a C_2/C_1 ratio of ~30%. At 1 atm, $\frac{3}{1}$ H_2/CO, and 203°C, the corresponding ratio found by Vannice and Garten (*9*) is ~40% for the 10% Ni/TiO_2 catalyst. The above overall agreement in activity and selectivity is encouraging and again confirms the validity of this combined UHV-catalysis approach using small-area single-crystal surfaces.

On the basis of our present method of turnover number calculation, one cannot exclude the possibility that the activity enhancement in $Ni/TiO_2(100)$ may be due to surface roughness (i.e., the effective surface area >0.38 cm^2). It is doubtful, however, that surface roughness can account for the full enhancement factor of 3.3–3.7 when the surface Ni coverage is only 5 Å [LEED shows that the growth of the Ni overlayer on $TiO_2(100)$ is near-epitaxial]. Further, if the enhancement were *purely* an area effect, the product distribution should remain unchanged.

The observed interaction between the deposited Ni and Ti^{3+} on TiO_2 and the negative charge on the Ni atoms may be the cause for the increase in the CO hydrogenation activity on Ni/TiO_2. Okamoto *et al.* (*41*) defined a parameter Δq to represent the extent of change in the electron density on Ni as a result of electron transfer between nickel and other component elements in the catalyst. They found that the adsorption equilibrium constant and the activity for hydrogenation are strongly dependent on Δq. It is known from metal–semiconductor studies (*42*) that charge transfer across the metal–semiconductor interface occurs upon the initial deposition of metal atoms on the semiconductor surface and is essentially complete after the formation of the first one or two metal monolayers. Therefore, the charge on the Ni atom will fall off rapidly from 0.1 e/atom at the interface (as measured in our experiments) to essentially neutral for Ni atoms at a few layers from the interface. If the charge on the Ni atoms is intimately related to the catalytic activity of the $Ni/TiO_2(100)$ system, then one would expect the activity enhancement to be confined to Ni thickness ~ a few layers and the activity to approach that of bulk Ni at large thickness. This is indeed what we observed (Fig. 8).

At small Ni thickness (e.g., 2 Å), Fig. 8 indicates that the methane yield is about the same as bulk Ni. The correlation between charge transfer and activity thus seems tenuous since the first 2 Å of Ni should have a larger negative charge per atom than subsequent Ni layers. This apparent discrepancy can be explained as follows. The growth of the Ni overlayer on $TiO_2(100)$ is near-epitaxial, but is by no means perfect. Isolated Ni atoms may form in one place and multiatom clusters in another. Methanation reaction studies using Ni–Cu alloys showed that the reaction requires ensembles of several Ni atoms to proceed (*43, 44*). Thus any surface inhomogeneity at low Ni coverage will reduce the effective concentration of active Ni sites and thus the methane yield. As the average Ni thickness increases, the concentration of active Ni sites increases, thereby resulting in an increased methane yield and the rising portion of Fig. 8. Data in Fig. 8 show that the methane yield of $Ni/TiO_2(100)$ acquires a maximum at an average Ni overlayer thickness of 5 Å (about 2½ layers). On the basis of the above discussion, we believe that the occurrence of this maximum is due to the combining effect of the variation of the charge state of surface Ni atoms and the effective concentration of active Ni sites as a function of the average Ni thickness.

In our experiments, we simulated the conditions leading to the strong metal–support-interactions (SMSI) observed in titania-supported catalysts (*6, 7*) by reducing the TiO_2 surface at 400°C before nickel deposition. It would be interesting to examine cases when such a strong interaction is expected to be absent (e.g., putting nickel onto a fully oxidized TiO_2 surface) or when the environment surrounding Ni is similar

to Ni/TiO_2(100), but the nickel atom is positively charged (e.g., nickel in nickel titanate). We are currently performing experiments with this objective.

SUMMARY

(1) There is an electron transfer from TiO_2(100) to Ni when Ni is deposited onto a reduced TiO_2(100) surface. The amount of charge transfer is ~0.1 electron per nickel atom when the nickel coverage is 1.0 Å.

(2) CO hydrogenation experiments have been performed on Ni(111) and Ni/TiO_2(100) at P_{H_2} = 60 Torr and P_{CO} = 20 Torr. The temperature variation of the methane turnover number follows an Arrhenius behavior with an activation energy of 26.7 kcal/mole for Ni(111) and 25.2 kcal/mole for 5 Å Ni/TiO_2(100).

(3) The methanation activity for Ni/TiO_2(100) is a function of the Ni coverage and attains a maximum at an average Ni thickness of 5 Å.

(4) The methane yield from 5 Å Ni/TiO_2(100) is about 3.3–3.7 times that from Ni(111) over the temperature range of 170–220°C, with an accompanying shift of the product distribution toward higher hydrocarbons.

ACKNOWLEDGMENTS

We would like to thank Dr. John Yates for useful discussions and for communicating to us results contained in Refs. (*22–25*) prior to publication. This work was supported by the Division of Materials Sciences, Office of Basic Energy Sciences, United States Department of Energy. The use of the Central Facilities of Northwestern University's Material Research Center, supported under the NSF-MRL program, facilitated this work.

REFERENCES

1. Schwab, G. M., Block, J., and Schultze, D., *Angew. Chem.* **71,** 101 (1958).
2. Schwab, G. M., *Angew. Chem.* **73,** 399 (1961).
3. Solymosi, F., *Catal. Rev.* **1,** 233 (1967).
4. Szabo, Z. G., and Solymosi, F., *Actes Congr. Int. Catal. 2nd 1960,* 1627 (1961).
5. Baddour, R. F., and Deibert, M. C., *J. Phys. Chem.* **70,** 2173 (1966).
6. Tauster, S. F., Fung, S. C., and Garten, R. L., *J. Amer. Chem. Soc.* **100,** 170 (1978).
7. Tauster, S. J., and Fung, S. C., *J. Catal.* **55,** 29 (1978).
8. Tauster, S. J., Fung, S. C., Baker, R. T. K., and Horsley, J. A., *Science* **211,** 1121 (1981).
9. Vannice, M. A., and Garten, R. L., *J. Catal.* **56,** 236 (1979).
10. Vannice, M. A., and Garten, R. L., *J. Catal.* **66,** 242 (1980).
11. Smith, J. S., Thrower, P. A., and Vannice, M. A., *J. Catal.* **68,** 270 (1981).
12. Bartholomew, C. H., Pannell, R. B., and Butler, J. L., *J. Catal.* **65,** 335 (1980).
13. Mustard, D. G., and Bartholomew, C. H., *J. Catal.* **67,** 186 (1981).
14. Horsley, J. A., *J. Amer. Chem. Soc.* **101,** 2870 (1979).
15. Chung, Y. W., and Weissbard, W. G., *Phys. Rev. B* **20,** 3456 (1979).
16. Bahl, M. K., Tsai, S. C., and Chung, Y. W., *Phys. Rev. B* **21,** 1344 (1980).
17. Somorjai, G. A., *Surf. Sci.* **89,** 496 (1979).
18. Sexton, B. A., and Somorjai, G. A., *J. Catal.* **46,** 167 (1977).
19. Dwyer, D. J., and Somorjai, G. A., *J. Catal.* **52,** 291 (1978).
20. Dwyer, D. J., and Somorjai, G. A., *J. Catal.* **56,** 249 (1979).
21. Castner, D. J., Blackadar, R. L., and Somorjai, G. A., *J. Catal.* **66,** 257 (1980).
22. Kelley, R. D., and Goodman, D. W., private communication.
23. Madey, T. E., Goodman, D. W., and Kelley, R. D., *J. Vac. Sci. Technol.* **16,** 433 (1979).
24. Goodman, D. W., Kelley, R. D., Madey, T. E., and Yates, J. T., Jr., *J. Catal.* **63,** 226 (1980).
25. Goodman, D. W., Kelley, R. D., Madey, T. E., and White, J. M., *J. Catal.* **64,** 479 (1980).
26. Krebs, H. J., and Bonzel, H. P., *Surf. Sci.* **88,** 269 (1979).
27. Bonzel, H. P., and Krebs, H. J., *Surf. Sci.* **91,** 499 (1980).
28. Krebs, J. H., and Bonzel, H. P., *Surf. Sci.* **99,** 570 (1980).
29. Kao, C. C., Tsai, S. C., Bahl, M. K., Chung, Y. W., and Lo, W. J., *Surf. Sci.* **95,** 1 (1980).
30. Chung, Y. W., Lo, W. J., and Somorjai, G. A., *Surf. Sci.* **64,** 588 (1977).
31. Lo, W. J., Chung, Y. W., and Somorjai, G. A., *Surf. Sci.* **71,** 199 (1978).
32. Bahl, M. K., *et al., J. Chem. Phys.* **66,** 5526 (1977).
33. Wagner, C. D., and Biloen, P., *Surf. Sci.* **35,** 82 (1973).
34. Shirley, D. A., *Chem. Phys. Lett.* **16,** 220 (1972).
35. Sayers, C. N., and Armstrong, N. R., *Surf. Sci.* **77,** 301 (1978).
36. Ferrer, S., and Somorjai, G. A., *Surf. Sci.* **94,** 41 (1980).

37. Richardson, J. T., and Crump, J. G., *J. Catal.* **57,** 417 (1979).
38. Kuo, H. K., Ganesan, P., and De Angelis, R. J., *J. Catal.* **64,** 303 (1980).
39. Vannice, M. A., *Catal. Rev. Sci. Eng.* **14,** 153 (1976).
40. Vannice, M. A., *J. Catal.* **44,** 152 (1976).
41. Okamoto, Y., Nitta, Y., Imanaka, T., and Teranishi, S., *J. Catal.* **64,** 397 (1980).
42. Spicer, W. E., Lindau, I., Skeath, P., Su, C. Y., and Chye, P., *Phys. Rev. Lett.* **44,** 420 (1980), and references therein.
43. Araki, M., and Ponec, V., *J. Catal.* **44,** 439 (1976).
44. Ponec, V., *Catal. Rev. Sci. Eng.* **18,** 151 (1978).